Physics and Chemistry of Minerals (2018) 45:523–531
https://doi.org/10.1007/s00269-017-0939-5

ORIGINAL PAPER

The stability of anhydrous phase B, $Mg_{14}Si_5O_{24}$, at mantle transition zone conditions

Liang Yuan[1,2] · Eiji Ohtani[1] · Yuki Shibazaki[3] · Shin Ozawa[1] · Zhenmin Jin[2] · Akio Suzuki[1] · Daniel J. Frost[4]

Received: 27 June 2017 / Accepted: 11 December 2017 / Published online: 27 December 2017

Abstract

The stability of anhydrous phase B, $Mg_{14}Si_5O_{24}$, has been determined in the pressure range of 14–21 GPa and the temperature range of 1100–1700 °C with both normal and reversal experiments using multi-anvil apparatus. Our results demonstrate that anhydrous phase B is stable at pressure–temperature conditions corresponding to the shallow depth region of the mantle's transition zone and it decomposes into periclase and wadsleyite at greater depths. The decomposition boundary of anhydrous phase B into wadsleyite and periclase has a positive phase transition slope and can be expressed by the following equation: $P(\mathrm{GPa}) = 7.5 + 6.6 \times 10^{-3} T$ (°C). This result is consistent with a recent result on the decomposition boundary of anhydrous phase B (Kojitani et al., Am Miner 102:2032–2044, 2017). However, our phase boundary deviates significantly from this previous study at temperatures < 1400 °C. Subducting carbonates may be reduced at depths > 250 km, which could contribute ferropericlase (Mg, Fe)O or magnesiowustite (Fe, Mg)O into the deep mantle. Incongruent melting of hydrous peridotite may also produce MgO-rich compounds. Anh-B could form in these conditions due to reactions between Mg-rich oxides and silicates. Anh-B might provide a new interpretation for the origin of diamonds containing ferropericlase–olivine inclusions and chromitites which have been found to have ultrahigh-pressure characteristics. We propose that directly touching ferropericlase–olivine inclusions found in natural diamonds might be the retrogressive products of anhydrous phase B decomposing via the reaction $(Mg,Fe)_{14}Si_5O_{24}$ (Anh-B) = $(Mg,Fe)_2SiO_4$ (olivine) + (Mg,Fe)O (periclase). This decomposition may occur during the transportation of the host diamonds from their formation depths of < 500 km in the upper part of the mantle transition zone to the surface.

Keywords Anhydrous phase B · Phase transition · Raman spectroscopy · High-*P* chromite · Diamond inclusions

Introduction

Anhydrous phase B (Anh-B), $Mg_{14}Si_5O_{24}$, was first synthesized by Herzberg and Gasparik (1989) in melting experiments that employed a chondritic chemical composition, at a condition of 2350 °C and 16.5 GPa. Kato and Kumazawa (1985) had previously synthesized a mineral with a molar ratio of Mg/Si ≈ 2.9 at near solidus conditions in melting experiments on forsterite. Although they considered it to be hydrous phase B $Mg_{12}Si_4O_{19}(OH)_2$, one of the dense hydrous magnesium silicates that was first synthesized by Ringwood and Major (1967), given the synthesis conditions it is more likely that Anh-B has been misidentified as hydrous phase B in their study. The crystal structure of Anh-B (Fig. 1) has been determined to have a space group *Pmcb*, with lattice parameters $a = 5.868(1)$, $b = 14.178(1)$, $c = 10.048(1)$ Å, $V = 835.9$ Å^3, and $Z = 2$ (Finger et al. 1989). The crystal structure can be conveniently described as comprising two

Electronic supplementary material The online version of this article (https://doi.org/10.1007/s00269-017-0939-5) contains supplementary material, which is available to authorized users.

✉ Liang Yuan
yuan.liang.s4@dc.tohoku.ac.jp

[1] Department of Earth and Planetary Materials Science, Graduate School of Science, Tohoku University, Sendai 980-8578, Japan

[2] School of Earth Sciences, China University of Geosciences, Wuhan 430074, China

[3] Frontier Research Institute for Interdisciplinary Sciences, Tohoku University, Sendai 980-8578, Japan

[4] Bayerisches Geoinstitut, University of Bayreuth, Bayreuth 95440, Germany

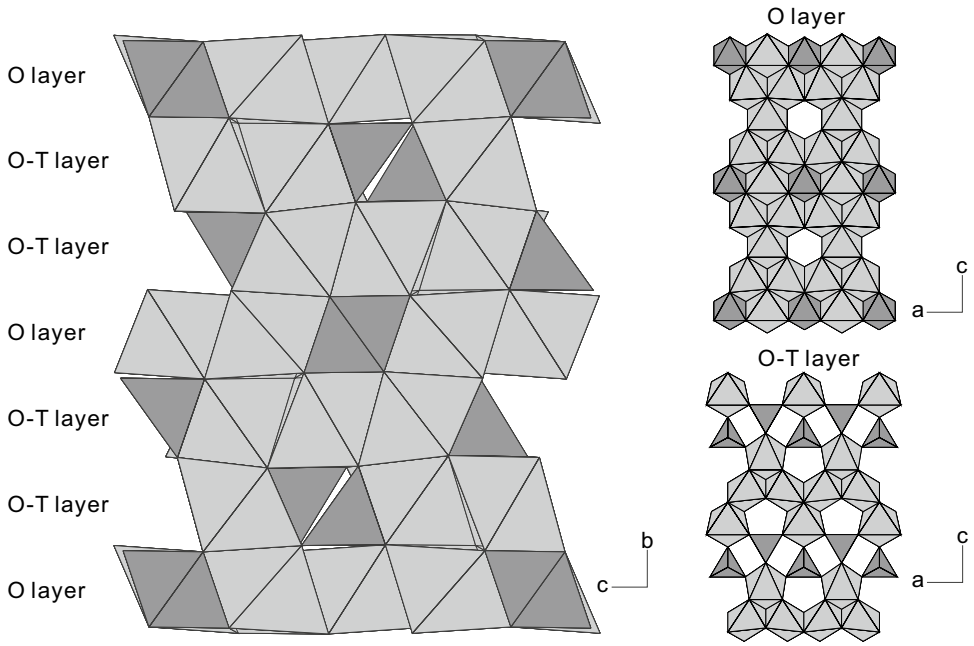

Fig. 1 Crystal structure of anhydrous phase B, $Mg_{14}Si^{VI}Si^{IV}_4O_{24}$. The crystal structure of Anh-B has a space group *Pmcb*, with lattice parameters $a = 5.868(1)$, $b = 14.178(1)$, $c = 10.048(1)$ Å, $V = 835.9$ Å^3, and $Z = 2$ (Finger et al. 1989). Its crystal structure can be conveniently described as being composed of two types of layers, one with edge-shared Mg and Si octahedra having the overall $Mg_{12}Si_2O_{16}$ stoichiometry (O layer), and the other with the Mg octahedra and Si tetrahedra and the stoichiometry of forsterite $Mg_{16}Si_8O_{32}$ (O-T layer)

types of layers, one with edge-shared Mg and Si octahedra having the overall $Mg_{12}Si_2O_{16}$ stoichiometry, and the other with Mg octahedra and Si tetrahedra with the stoichiometry of forsterite $Mg_{16}Si_8O_{32}$.

Melting experiments of both hydrous and anhydrous pyrolite have shown the presence of Anh-B near the solidus (Litasov et al. 2001; Litasov and Ohtani 2002). These experiments indicate that there is an expansion of the stability of Anh-B under wet conditions. It is noteworthy that below the solidus, Anh-B has been shown to coexist with garnet in the absence of ringwoodite or wadsleyite. Under certain *P–T* conditions, ringwoodite and wadsleyite apparently transform into Anh-B and garnet (Litasov et al. 2001; Litasov and Ohtani 2002). Ganguly and Frost (2006) determined the phase transition boundary of the reaction Mg_2SiO_4 (forsterite) + MgO (periclase) = $Mg_{14}Si_5O_{24}$ (Anh-B) in the pressure range of 9–12.5 GPa, and the temperature range 900–1600 °C. The reaction was confirmed by first-principles calculations (Ottonello et al. 2010). Ganguly and Frost (2006) also proposed that, under certain *P–T* conditions in a subduction zone, forsterite Mg_2SiO_4 may decompose into Anh-B $Mg_{14}Si_5O_{24}$ and stishovite SiO_2 or akimotoite $MgSiO_3$ based on thermodynamic calculations.

Anh-B might be an important phase in the deep mantle as MgO-rich compounds might be produced through incongruent melting of both anhydrous and hydrous peridotite. Studies of the MgO–SiO_2–H_2O system indicate that melting of hydrous phases at high pressures and temperatures could lead to the formation of liquids that are concentrated in MgO (Inoue and Sawamoto 1992; Stalder et al. 2001; Mibe et al. 2002; Melekhova et al. 2007). Experiments on a serpentine starting material, for example, resulted in the generation of liquids with an MgO/SiO_2 weight ratio close to 2 at 9 GPa (Stalder et al. 2001). An MgO/SiO_2 weight ratio of typically 6–9 in liquid was obtained using a Mg-rich starting composition with an MgO/SiO_2 weight ratio = 3.8 at pressures of 11–13.5 GPa and temperatures between 1000 and 1350 °C (Melekhova et al. 2007). Furthermore, the breakdown of hydrous phase D $MgSi_2O_4(OH)_2$ at 22–32 GPa, 1300–1450 °C produced a liquid with an MgO/SiO_2 weight ratio of between 2 and 5 (Ghosh and Schmidt 2014). Therefore, hydrous melting could play a crucial role in the redistribution of silica between the melt and solid residue at high-pressure and high-temperature conditions. In subduction zones within the deep mantle, dehydration melting of subducted hydrous phases might result in the formation of MgO-rich melts. Melts with MgO-rich signatures might also be formed near the 410-km discontinuity, where dehydration melting might occur due to a sharp contrast of water solubility across the discontinuity (Litasov and Ohtani 2002; Bercovici and Karato 2003).

An additional scenario we propose here is that the reduction of subducted carbonates in the deep mantle might also produce abundant MgO leading to the formation of Anh-B. Silicates at high pressures can incorporate large amount of ferric iron (McCammon 1997; Frost et al. 2004; Rohrbach et al. 2007). Metallic iron could be saturated in the deep mantle because of charge disproportionation where Fe^{2+} (silicates) → Fe^{3+} (silicates) + Fe^0 (metal). The experimental evidences are in line with the discovery of metallic iron phases included in natural diamonds presumably originated from the mantle transition zone or uppermost lower mantle (Smith et al. 2016). Subducted carbonates might become unstable if they are exposed to such a reducing

environment where metals probably become stable. The interaction between carbonates and (Fe,Ni)-metal via the reaction $MgCO_3 + 2(Fe,Ni)^0 = 3(Fe,Ni,Mg)O + C$, as has been experimentally demonstrated by Rohrbach and Schmidt (2011), can potentially result in the formation of ferropericlase (Mg,Fe)O in the surrounding mantle. An association containing magnesiowustite (Fe,Mg)O was produced in experiments performed to study the reduction of subducted $(Mg,Ca)CO_3$ at the mantle–slab interaction zone (Palyanov et al. 2013). The ferropericlase (Mg,Fe)O or magnesiowustite (Fe,Mg)O formed may then be partially consumed by MgO-deficient components, such as pyroxene and garnet, in the ambient peridotitic mantle. However, some amount of Anh-B could still be formed if sufficient initial carbonate were present. Within ultrabasic systems the interaction between olivine $(Mg,Fe)_2SiO_4$, and ferropericlase (Mg,Fe)O or magnesiowustite (Fe,Mg)O produced by the reduction of carbonates is even more plausible. The subduction of magnesite-bearing dunite thus might be an optimal source for the formation of Anh-B in the transition zone. In conclusion, mainly two processes, i.e., dehydration melting and the reduction of subducted carbonates, can locally render an enrichment of MgO in the deep mantle.

As it is present on the peridotite liquidus (Herzberg and Zhang 1996; Litasov et al. 2001; Litasov and Ohtani 2002), Anh-B might have also crystallized and accumulated at depths corresponding to the shallow part of the mantle transition zone, during cooling of a deep global magma ocean in Earth's early history. Thus, Anh-B might have been a possible constituent together with phases such as wadsleyite and garnet in the shallow part of the mantle transition zone in the Hadean, although such magma ocean cumulates may have mixed back into the mantle by later stages of vigorous mantle convection.

Although the Earth has a pyrolitic bulk composition, considering that the distribution of mantle compositions is likely spatially and temporally heterogeneous, Anh-B might form in depths where there is an enrichment of MgO or a depletion of SiO_2. There is, however, some uncertainty concerning the stability of Anh-B over a wider range of *P–T* conditions. In this study, the phase stability of Anh-B was constrained by high-pressure and high-temperature experiments in the pressure range of 14–21 GPa and the temperature range of 1100–1700 °C using multi-anvil apparatus.

Experimental methods

Starting material

The starting composition was synthesized from a mixture of MgO and SiO_2 with a stoichiometric composition necessary to produce Anh-B, $Mg_{14}Si_5O_{24}$ (Finger et al. 1989). All the oxides were dried in an ambient-pressure furnace at 1000 °C for 12 h to remove the absorbed water before weighting and mixing. The oxide mixture of MgO and SiO_2 were ground in an agate mortar under ethanol for about 3 h. After that, the homogeneous mixture of MgO and SiO_2 oxides was annealed in an ambient-pressure furnace at 1400 °C for 24 h to synthesize an assemblage of forsterite and periclase. An analysis of X-ray powder diffraction confirmed that the product was composed of only two phases, forsterite and periclase. The assemblage of forsterite and periclase was crushed and ground under ethanol to make a homogeneous mixture. Finally, the entire mixture was stored in an ambient-pressure oven at 130 °C before its use in high-pressure and high-temperature experiments. The assemblage of forsterite and periclase was tightly packed into a metal capsule for normal, i.e., synthesis or forward experiments.

For reversal runs, pre-synthesized Anh-B was used as a starting material. Anh-B was synthesized at 1200 °C, 12 GPa for 12 h, using the forsterite and periclase starting composition employed in normal experiments. X-ray diffraction and Raman spectroscopy analysis indicated that the run product of the Anh-B-synthesis experiment was composed of nearly single-phase Anh-B.

Multi-anvil apparatus

High-pressure and high-temperature experiments were carried out using a Kawai-type multi-anvil apparatus driven by a 3000-ton DIA-type guide-block–uniaxial press system at Tohoku University (Ohtani et al. 1998). Hardened tungsten carbide cubes (Fujiloy, TF05) with 3 mm truncation edge length (TEL) and 26 mm edge length were used as the second-stage anvils for experiments. ZrO_2 was used as a pressure medium. Pyrophyllite gaskets were placed between cubes to seal the extrusion of the pressure medium. TiB_2-doped BN furnaces were used for heating. The samples, contained in Pt capsules of ~ 1.5 mm length and ~ 0.8 mm diameter, were insulated from the furnaces by MgO sleeves. A $W_{97}Re_3$–$W_{75}Re_{25}$ thermocouple was inserted in the center via pre-drilled holes and electrically insulated from the furnace by aluminum tubes. Details of the similar cell assembly were given by Litasov and Ohtani (2005). Pressure was calibrated against the reaction of forsterite–wadsleyite (14.3 GPa, 1400 °C, Morishima et al. 1994), wadsleyite–ringwoodite (18.6 GPa, 1200 °C, Suzuki et al. 2000), and the breakdown of ringwoodite to perovskite and periclase (23.3 GPa, 1400 °C, Fei et al. 2004). The pressure uncertainty was estimated at ± 1 GPa (Litasov et al. 2001). Additional experiments were made using a multi-anvil apparatus driven by a 1000-ton Walker-type guide-block–uniaxial press system installed at the China University of Geosciences. Tungsten carbide cubes with 3 or 5 mm TEL and 26 mm edge length were

used as the second-stage anvils for experiments. Details of the assemblies were given by Zhang et al. (2013, 2016). Pressure was calibrated based on the forsterite–wadsleyite (14.6 GPa, 1400 °C, Katsura et al. 2004) and wadsleyite–ringwoodite (20 GPa, 1400 °C, Suzuki et al. 2000) and the breakdown of ringwoodite to perovskite and periclase (23.1 GPa, 1600 °C, Fei et al. 2004). We only employed the experimental results from the multi-anvil apparatus driven by the DIA-type guide-block–uniaxial press system to constrain the phase transition boundary to avoid incorporating errors arising from using different multi-anvil apparatus. For all experiments, pressures were applied first to achieve the target ram loads, then temperature was increased to the desired values. Samples were heated at given pressures for 2–29 h depending on the experimental temperatures. The experiments were quenched by directly turning off the heating power to the furnaces at high pressures, and samples were recovered after releasing pressure.

Analytical procedures

At the end of each experiment, the sample together with the surrounding metal capsule was recovered from the compressed pressure medium and mounted in epoxy resin. Then the sample was carefully ground to expose a cross-section through the center. The final surface of the sample was polished with diamond pastes (3, 1 and 0.25 μm). Finally, the polished sample was coated with carbon for further micro-analysis. A field-emission scanning electron microscope (FE-SEM) (Quanta 2000-type) coupled with a Link energy-dispersive spectroscopy detector or a JSM 5410LV-type of SEM coupled with an EDS detector was used to study the microstructure and chemical composition of the recovered samples.

Analysis with micro-Raman spectroscopy was performed using a JASCO NRS-4100 Raman spectrometer installed at Tohoku University with 532-nm excitation of an argon ion laser, Czerny–Turner mount single monochromator and air-cooled Peltier CCD detector. The laser power at the sample surface was set approximately at 6 mW to avoid overheating the sample and to decrease the effect of fluorescence. The laser beam diameter was about 1 μm. Raman data were collected through repeated exposures of 60 s, one or two accumulations for each measurement. The corresponding spectral resolution was 0.25 cm^{-1}. Raman spectra were collected in the low-frequency range between 100 and 1200 cm^{-1} for phase identification and in the high-frequency range between 2800 and 3600 cm^{-1} to detect for the possible incorporation of hydrogen into the mineral crystal structures. For the collection of Raman spectra for Anh-B, relatively large crystals (~ 100 μm) of Anh-B with well-polished surfaces were exposed to the laser beam in order to ensure the quality of the spectra.

Results and discussion

Raman spectra of anhydrous phase B

Representative Raman spectra measured for Anh-B from our experiments are shown in Fig. 2. Anh-B has 86 atoms in its unit cell so that there are 255 [(3 × 86) − 3] vibrational modes. The irreducible representation of the vibrational mode symmetry for the space group *Pmcb* is as follows:

$$\Gamma = 35A_g + 25B_{1g} + 25B_{2g} + 35B_{3g} + 28A_u + 41B_{1u} + 41B_{2u} + 28B_{3u}.$$

Of these the Raman-active modes are $35A_g + 25B_{1g} + 25B_{2g} + 35B_{3g}$. Thus, a total of 120 vibrational peaks are expected in the Raman spectrum of Anh-B. The Raman shifts were determined within an uncertainty of 0.5 cm^{-1}. The number of observed Raman modes is much smaller than that predicted because of the low intensity of

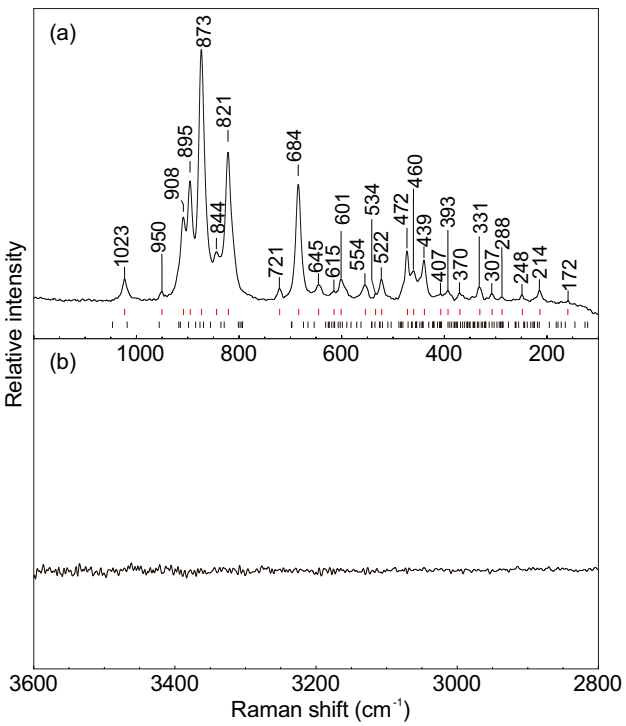

Fig. 2 Typical Raman spectra of anhydrous phase B in the low-frequency range between 100 and 1200 cm^{-1} (**a**), and the high-frequency range between 2800 and 3600 cm^{-1} (**b**) which does not show any distinctive peak related to OH stretching vibrations. Two sets of short lines below the spectrum in **a** denote the peak frequencies, with the red lines representing the experimental observation, the black lines the ab initio calculation result from Ottonello et al. (2010)

some external vibrational modes. The observed peaks are distributed in the frequency range of 172–1023 cm^{-1}, with the strongest one typically located at 873 cm^{-1}. Several other peaks with strong intensity can be found at the locations of 684, 821, 873, 895, and 908 cm^{-1}(Fig. 2a). The peak positions observed in this study are comparable with those reported in Ohtani et al. (2001). Vibrational frequencies for Anh-B were calculated by Ottonello et al. (2010) based on ab initio calculations. The measured spectrum is in general agreement with that of the theoretical calculation, although a significant number of the calculated vibrational peaks predicted at lower frequencies cannot be distinguished within the measured spectrum. No distinct peak appears to be related to OH stretching vibrations in the high-frequency range between 2800 and 3600 cm^{-1} for the Anh-B in our experiments (Fig. 2b), whereas in the case of hydrous phase B, distinctive peaks were observed in the high-frequency region (Finger et al. 1989).

Determination of phase transition boundary

Experiments were conducted in the pressure range of 14–21 GPa, and the temperature range 1100–1700 °C using the DIA-type and Kawai-type multi-anvil apparatus. Chemical compositions of phases were determined by SEM coupled with EDS. Raman spectroscopy was used to distinguish α-, β-, and γ-Mg_2SiO_4 and to identify Anh-B in our run products. Electron microprobe analysis of Anh-B (run products at 17 GPa, 1500 °C) yielded a Mg/Si ratio of 2.82 ± 0.02 for the average of 20 spot analyses, which was the same value as that reported by Finger et al. (1989) for Anh-B. Analyses of the chemical composition of Anh-B with SEM-EDS also yielded a Mg/Si ratio of 2.8.

The experimental conditions and observed run products are summarized in Table 1. Typical back-scattered electron images of the run products are presented in Fig. 3. At a temperature of 1500 °C, Anh-B was found to be stable below 17 GPa (Fig. 3a). However, Anh-B was not found at higher pressures, i.e., > 18 GPa (Fig. 3b). SEM images show quite clearly that periclase and wadsleyite coexist in the absence of Anh-B at 1500 °C and 18 GPa. Thus, the

Table 1 Experimental conditions and results

Exp. no.	Starting material[a]	Pressure (GPa)	Temperature (°C)	Duration (h)	Results
R585	1	17	1500	5	Anh-B (Wd, Pc)
R591	1	15	1300	10	Anh-B (Wd, Pc)
R594	1	21	1450	8	Rw, Pc
R602	1	19	1500	3	Wd, Pc
R603	1	18	1500	3	Wd, Pc
R620	1	19	1100	12	Rw, Pc
R625	1	18	1100	4	Rw, Pc
R626	1	16	1700	2	Anh-B (Wd, Pc)
T2273	1	19	1300	2	Wd, Pc
T2277	1	18	1300	2	Wd, Pc
T2278	1	17	1300	2	Wd, Pc
T2279	1	17	1500	2	Anh-B (Wd, Pc)
T2281	1	17.5	1500	2	Anh-B (Wd, Pc)
T2284	1	18	1500	2	Wd, Pc
T2287	1	17	1300	8	Wd, Pc
T2288	1	16	1300	4	Anh-B (Wd, Pc)
T2290	1	16.5	1300	8	Wd, Pc
T2293	1	15	1100	9	Wd, Pc
T2297	1	14	1100	5	Anh-B (Wd, Pc)
T2302	1	14.5	1100	13	Anh-B (Wd, Pc)
T2307	2	16.7	1400	8	Anh-B, Wd, Pc
T2312	2	15.7	1200	29	Wd, Pc
T2313	1	18	1600	2	Anh-B, Wd, Pc

Wd wadsleyite, *Rw* ringwoodite, *Anh-B* anhydrous phase B, *Pc* periclase

[a]Starting materials are 1, Fo + Pc and 2, Anh-B + Fo + Pc. Unstable phases present in each run are listed in the parenthesis. Experiments labeled T and R were conducted on a 3000-ton DIA-type and a 1000-ton Walker-type multi-anvil apparatus, respectively

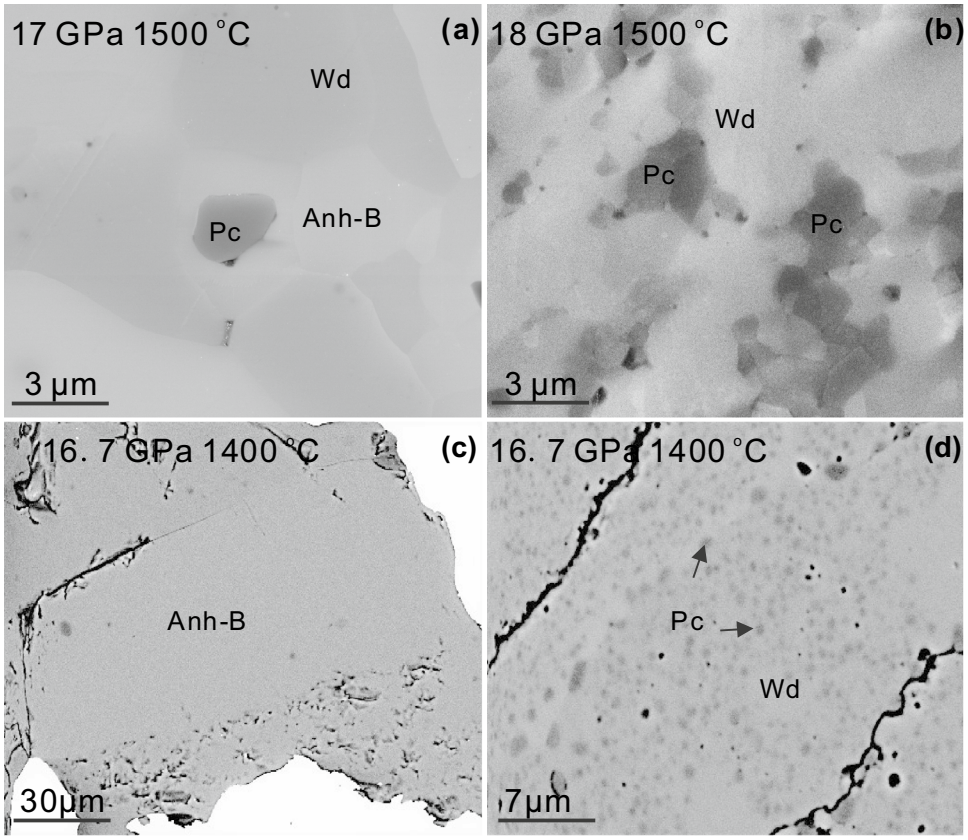

Fig. 3 Back-scattered electron images from a scanning electron microscope: **a** run products from 17 GPa, 1500 °C, where wadsleyite and periclase have reacted to form Anh-B although some reactants remain due to sluggish reaction rates; **b** run products from 18 GPa, 1500 °C, where wadsleyite and periclase coexist beyond the stability field of Anh-B; **c, d** run products from 16.7 GPa, 1400 °C, showing the results of a reversal experiment where pre-synthesized Anh-B has been packed at the top (i.e., high-temperature side) of the capsule and has remained stable (**c**), whereas **d** shows an enlargement of the bottom end (i.e., low-temperature side) of the same capsule where Anh-B has decomposed into wadsleyite and periclase

phase transition boundary of Anh-B = Wd + Pc was bracketed between 17 and 18 GPa at 1500 °C. An additional run was then conducted at 17.5 GPa to more tightly bracket the pressure of the phase transition to within 0.5 GPa. Due to the slow reaction kinetics of solid–solid phase transitions under dry conditions, complete equilibrium was not achieved during the formation of Anh-B, as unreacted starting materials remained in the run products. At the highest temperature investigated, 1700 °C, it was possible to acquire a nearly single-phase assemblage of Anh-B with a heating duration of ~ 2 h. Longer heating durations were routinely employed at lower temperatures, for instance, at a temperature of 1200 °C heating durations were up to 29 h, in order to counteract the effect of sluggish reaction rates. The experimental results are summarized in Fig. 4 as a phase diagram. The phase transition boundary is constrained by both normal and reversal experiments. Based on our experiments, we bracketed the phase transition boundary between 14.5 and 15 GPa at 1100 °C, 16 and 16.5 GPa at 1300 °C, and 17.5 and 18 GPa at 1500 °C, respectively. Therefore, the Clapeyron slope of the phase transition boundary can be calculated to be ~ 6.6 MPa/°C using the "best fit" curve to the experimental data.

We conducted two reversal experiments to verify the equilibrium phase relations obtained from forward experiments. For the reversal experiments, we selected three large pieces of pre-synthesized Anh-B aggregates and packed them at the bottom, middle, and top of a capsule. The interstitial spaces among the three large Anh-B aggregates were filled by packing the powder of forsterite and periclase used in the normal experiments. After the experiments were performed, the recovered samples were examined to see whether or not the Anh-B had transformed into Wd + Pc. For the experiment at 1400 °C and 16.7 GPa, run for 8 h (T2307), pre-synthesized Anh-B was found to be stable within the upper region of the capsule (Fig. 3c), where the temperature was expected to be higher than at the other end of the capsule as the top of the capsule was closer to the center of furnace. At the lower part of the capsule, we found that the pre-synthesized Anh-B aggregate decomposed into wadsleyite and periclase, and no Anh-B was detected in the area where the original forsterite and periclase mixture had been packed. The decomposition texture of Anh-B can be readily distinguished from that of unreacted Wd and Pc (Fig. 3d). Anh-B decomposition texture was characterized by the small round appearance of periclase homogeneously distributed among larger grains of wadsleyite. Unreacted Wd and Pc crystals, on the other hand, generally have more equal grain sizes and are of polygonal shape. The temperature at the top of the capsule, which was that measured by the thermocouple of 1400 °C, was within the stability field of Anh-B; whereas the temperature at the bottom of the

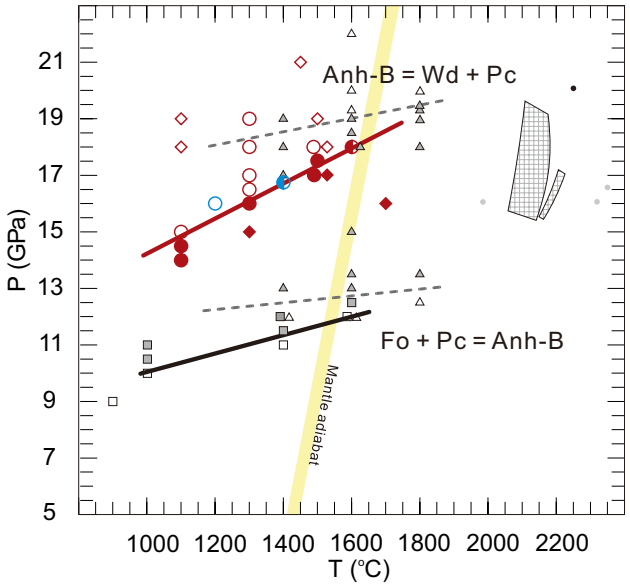

Fig. 4 *P–T* diagram showing the experimentally determined stability of anhydrous phase B. The solid symbols represent experiments where Anh-B is stable; the open symbols represent experiments where Anh-B is unstable. The red and blue colors indicate forward experiments and reversal experiments, respectively. The circle and diamond symbols indicate experiments conducted in this study with a DIA-type and a Walker-type multi-anvil apparatus, respectively. The thick red curve shows the decomposition boundary of Anh-B = Wd + Pc determined from this study. The small triangles and dash curves are taken from Kojitani et al. (2017). The squares and solid black curve are taken from Ganguly and Frost (2006). The small black dot denotes the first synthesis of Anh-B in the experiments by Kato and Kumazawa (1985). The small grey dot and the hatched areas are conditions where Anh-B has been identified in melting experiments performed using peridotitic systems (Herzberg and Gasparik 1989; Herzberg and Zhang 1996; Litasov and Ohtani 2002). Also shown for comparison is a mantle adiabat (Katsura et al. 2010) depicted by the yellow thick curve

capsule, which is expected to be lower than 1400 °C due to the temperature gradient, was within the stability field of wadsleyite and periclase. We expect the temperature differences between the top and bottom of the capsule to be < 50 °C based on previous experiments where a similar cell assembly was employed (Litasov and Ohtani 2002). Thus, the experiment at 1400 °C and 16.7 GPa, encompassed conditions that spanned the Anh-B = Wd + Pc equilibrium. A second reversal experiment was conducted at 1200 °C and 15.7 GPa for 29 h. Anh-B was found to be unstable, and it decomposed into wadsleyite and periclase both within the top and bottom regions of the capsule (Fig. S1). The results from the reversal experiment are consistent with that of the normal experiments. Based on the results of both normal and reversal experiments, it can be confirmed that the decomposition reaction of Anh-B = Wd + Pc possesses a positive slope, and the phase boundary can be expressed by the following equation: $P(\mathrm{GPa}) = 7.5 + 6.6 \times 10^{-3} T$ (°C).

The decomposition pressures for the equilibrium Anh-B = Wd + Pc were determined recently to be located at ~ 19 GPa at 1600 °C, and ~ 18.5 GPa at 1400 °C by Kojitani et al. (2017), which is 1–2 GPa higher than the results in this study. Our experimental data deviate significantly from the model of Kojitani et al. (2017) by ~ 3 GPa below 1400 °C. The equilibrium reaction of Fo + Pc = Anh-B determined by Kojitani et al. (2017) is also placed at slightly higher pressure by 0.5–1.5 GPa than that determined by Ganguly and Frost (2006). These discrepancies might be induced by different pressure calibration methods, and perhaps pressure dropping during heating that typically occurs in multi-anvil experiments. A precise determination of the phase transition boundary might also be hampered by the slow reaction kinetics at low temperatures particularly under dry conditions. Between 1100–1300 °C, we did not find Anh-B at pressures higher than 15–16 GPa with experimental heating durations of 8–9 h. On the other hand, the growth of Anh-B from forsterite and periclase was observed at lower temperatures within shorter heating durations (Ganguly and Frost 2006). The absence of Anh-B in our low temperature experiments therefore cannot be ascribed to slow reaction kinetics. The decomposition of Anh-B at 15.7 GPa, 1200 °C in one of the reversal experiments further suggests that the equilibrium Anh-B = Wd + Pc should preserve a large decomposition slope.

The stability of Anh-B and effects of minor elements

The stability of Anh-B is constrained by the equilibrium Fo + Pc = Anh-B as the lower boundary, and the equilibrium Anh-B = Wd + Pc as the upper boundary. Anh-B has been shown to be stable near the solidus of peridotitic compositions in previous experiments (Kato and Kumazawa 1985; Herzberg and Gasparik 1989; Herzberg and Zhang 1996; Litasov and Ohtani 2002; Liebske and Frost 2012). The stability of Anh-B from previous melting experiments is consistent with the stability field provided in this study. Along a typical mantle geotherm (Katsura et al. 2010), Anh-B will be stable up to a depth of approximately 500 km, corresponding to the shallow part of the mantle transition zone.

Anh-B has been mainly synthesized in MgO-rich compositions, or as a result of incongruent melting of Mg_2SiO_4. At conditions of 2280 °C and 20 GPa, Anh-B was found to coexist with melt in melting experiments on Mg_2SiO_4 (Kato and Kumazawa 1985). At conditions of 2350 °C and 16.5 GPa, Anh-B was also found to be stable in melting experiments performed using a chondritic starting material (Herzberg and Gasparik 1989). The stability of Anh-B might also be affected by other elements, such as Fe, Al, and Cr. A remarkable feature of Fe-bearing Anh-B is that Fe has been found to partition strongly into the M3 site, i.e., the octahedral site sharing two edges with Si octahedra

(Hazen et al. 1992). The substitution of the larger Fe for Mg in the M3 site decreases the lattice strain, and thus has the potential to stabilize the crystal structure of Anh-B. Melting experiments on anhydrous peridotite KLB-1 suggested that Anh-B was restricted to conditions near the liquidus at 2100–2200 °C, 15–17 GPa (Herzberg and Zhang 1996). Ohtani et al. (1998) observed Anh-B in experiments performed to study the melting of Fe-bearing olivine, with a FeO content of 10 wt%. However, in melting experiments in a more Fe-rich peridotitic system, Anh-B was not detected over the entire pressure and temperature range (Ohtani et al. 1995). This appears to contrast with the proposal of Hazen et al. (1992) based on the study of crystal chemistry of Fe-bearing Anh-B, that the substitution of Fe for Mg should significantly extend the stability of Anh-B. The partitioning coefficients between Anh-B and silicate melt for a number of minor components such as Cr_2O_3, Al_2O_3, MnO and NiO are quite large (Herzberg and Zhang 1996). A recent study indicated that up to 5.37 wt% Cr_2O_3 can be incorporated into the crystal structure of Ann-B through the $2Cr^{3+} = Mg^{2+} + Si^{4+}$ coupled substitution (Bindi et al. 2016). It seems that the distinctive M3 octahedron plays a crucial role in facilitating the incorporation of minor elements into the crystal structure of Anh-B. The presence of cations with large ionic radii, on the other hand, might help to stabilize the structure of Anh-B.

Implications for natural high-pressure chromitites and diamond inclusions

Abundant novel high-pressure minerals have been discovered in ophiolitic chromitites (Yang et al. 2007). The natural chromitite, previously thought to be a product of melt-peridotite reaction at very low pressure, was proposed to have a history of mantle transition zone metamorphism in order to explain the characteristics of the high-pressure phases found (Griffin et al. 2016). The natural high-*P* chromitite is mainly composed of chromite ($MgCr_2O_4$) and olivine (Mg_2SiO_4). It is thus highly depleted in SiO_2. $MgCr_2O_4$ decomposes into MgO and Cr_2O_3 between 12 and 15 GPa, < 1100 °C (Ishii et al. 2015). Therefore, olivine and chromite might be replaced by a paragenesis containing Anh-B at *P*–*T* conditions corresponding to the stability field of Anh-B. Cr-bearing Anh-B was indeed observed in the system $MgCr_2O_4$–Mg_2SiO_4 at 12 GPa and 1600 °C (Bindi et al. 2016). Chemical analysis showed that there is a gradual chemical composition change at the interface between chromite and olivine in the high-*P* chromitite (Xiong et al. 2015), which might be a result of the reaction between Mg_2SiO_4 and $MgCr_2O_4$. However, we are unaware of any report of either Anh-B or the retrogression products of Anh-B in natural high-*P* chromite occurrences. If either Anh-B or its retrogression products were to be found at the interface between olivine and chromite, this might shed light on the origin of natural high-*P* chromitites based on the experimental results from this study.

Stachel et al. (2000) reported an association of ferropericlase–olivine included in natural diamonds from the Kankan distinct, Guinea. A similar paragenesis has also been reported in diamonds from Juina area, Brazil (Hayman et al. 2005, as shown in Fig. 6d in their report). The olivine–periclase touching inclusions show varied chemical composition and might be derived from the stability field of olivine or the 660-km seismic discontinuity, where both ringwoodite and periclase are stable phases (Stachel et al. 2000). Interestingly, Stachel et al. (2000) concluded that crystallization of ferropericlase together with olivine possibly occurred from a magnesite-bearing dunitic source. This proposal is consistent with the recent growing body of experimental results showing that MgO can be produced from the interaction between subducted carbonates and metal-saturated mantle at high pressures and high temperatures as discussed in the previous section (Rohrbach and Schmidt 2011; Palyanov et al. 2013; Martirosyan et al. 2016). Here we put forward one further proposal that the ferropericlase–olivine pairs in natural diamonds might be retrogression products of Anh-B via the decomposition reaction Anh-B = Fo + Pc during the transportation of diamond from the deep mantle to the surface. Our experimental results put a constraint on the origin of the diamond at a depth less than 500 km, corresponding to the shallow part of the mantle transition zone. Diamonds and Anh-B might crystallize almost at the same time and location through the successive reactions (1) $MgCO_3 + 2(Fe,Ni)^0 = 3(Fe,Ni,Mg)O + C$ (diamond) and (2) $(Fe,Ni,Mg)O + Mg_2SiO_4 = (Fe,Ni,Mg)_{14}Si_5O_{24}$ (Anh-B). Based on this scenario, it is plausible that the crystallized Anh-B grains might be occasionally entrapped by diamonds which are produced in the same reaction. During mantle upwelling, Anh-B included in diamonds can disassociate into a paragenesis of olivine and periclase. To confirm this assumption, further work on phase relations in magnesite-bearing peridotitic systems or magnesite + olivine assemblages under reducing conditions are necessary.

Acknowledgements E.O. acknowledges the financial support from the Japan Society for the Promotion of Science (No. 15H05748). A.S. acknowledges the financial support from the Ministry of Education, Science, Sports and Culture, Grant-in-Aid for Scientific Research on Innovative Areas (15H05826, 15H05828, and 15K21712). Z.J. thanks the financial support from the National Natural Science Foundation of China (41174076). L.Y. is supported by the International Joint Graduate Program in Earth and Environmental Science (GP-EES), Tohoku University. D.F. acknowledges DFG funding of the International Research and Training Group "Deep Volatile Cycles".

References

Bercovici D, Karato S-i (2003) Whole-mantle convection and the transition-zone water filter. Nature 425:39–44

Bindi L et al (2016) Chromium solubility in anhydrous Phase B. Phys Chem Miner 43:103–110

Fei Y, Orman JV, Li J, Westrenen WV, Sanloup C, Minarik W, Hirose K, Komabayashi T, Walter M, Funakoshi K (2004) Experimentally determined postspinel transformation boundary in Mg_2SiO_4 using MgO as an internal pressure standard and its geophysical implications. J Geophys Res. https://doi.org/10.1029/2003JB002562

Finger L et al (1989) Crystal chemistry of phase B and an anhydrous analogue: implications for water storage in the upper mantle. Nature 341:140–142

Frost DJ et al (2004) Experimental evidence for the existence of iron-rich metal in the Earth's lower mantle. Nature 428:409–412

Ganguly J, Frost DJ (2006) Stability of anhydrous phase B: experimental studies and implications for phase relations in subducting slab and the X discontinuity in the mantle. J Geophys Res Solid Earth 111:B06203

Ghosh S, Schmidt MW (2014) Melting of phase D in the lower mantle and implications for recycling and storage of H_2O in the deep mantle. Geochim Cosmochim Acta 145:72–88

Griffin W et al (2016) Mantle recycling: transition zone metamorphism of Tibetan ophiolitic peridotites and its tectonic implications. J Petrol 57:655–684

Hayman PC et al (2005) Lower mantle diamonds from Rio Soriso (Juina area, Mato Grosso, Brazil). Contrib Miner Petrol 149:430–445

Hazen RM et al (1992) Crystal chemistry of Fe-bearing anhydrous phase B: implications for transition zone mineralogy. Am Miner 77:217–220

Herzberg C, Gasparik T (1989) Melting experiments on chondrite at high pressures: stability of anhydrous Phase B. Eos 70:484

Herzberg C, Zhang J (1996) Melting experiments on anhydrous peridotite KLB-1: compositions of magmas in the upper mantle and transition zone. J Geophys Res Solid Earth 101:8271–8295

Inoue T, Sawamoto H (1992) High pressure melting of pyrolite under hydrous condition and its geophysical implications. In: Syono Y, Manghnani MH (eds) High-pressure research: application to earth and planetary sciences. Terra, Tokyo and AGU, Washington, DC, pp 323–331

Ishii T et al (2015) High-pressure high-temperature transitions in $MgCr_2O_4$ and crystal structures of new $Mg2Cr_2O_5$ and post-spinel $MgCr_2O_4$ phases with implications for ultrahigh-pressure chromitites in ophiolites. Am Miner 100:59–65

Kato T, Kumazawa M (1985) Incongruent melting of Mg_2SiO_4 at 20 GPa. Phys Earth Planet Inter 41:1–5

Katsura T, Yamada H, Nishikawa O, Song M, Kubo A, Shinmei T, Yokoshi S, Aizawa Y, Yoshino T, Walter MJ, Ito E (2004) Olivine–wadsleyite transition in the system $(Mg,Fe)_2SiO_4$. J Geophys Res 109:B02209. https://doi.org/10.1029/2003JB002438

Katsura T, Yoneda A, Yamazaki D, Yoshino T, Ito E (2010) Adiabatic temperature profile in the mantle. Phys Earth Planet Inter 183:212–218

Kojitani H et al (2017) Experimental and thermodynamic investigations on the stability of $Mg_{14}Si_5O_{24}$ anhydrous phase B with relevance to Mg_2SiO_4 forsterite, wadsleyite, and ringwoodite. Am Miner 102:2032–2044

Liebske C, Frost DJ (2012) Melting phase relations in the MgO–$MgSiO_3$ system between 16 and 26 GPa: implications for melting in Earth's deep interior. Earth Planet Sci Lett 345:159–170

Litasov K, Ohtani E (2002) Phase relations and melt compositions in CMAS–pyrolite–H_2O system up to 25 GPa. Phys Earth Planet Inter 134:105–127

Litasov K, Ohtani E (2005) Phase relations in hydrous MORB at 18–28 GPa: implications for heterogeneity of the lower mantle. Phys Earth Planet Inter 150:239–263

Litasov K et al (2001) Melting relations of hydrous pyrolite in CaO–MgO–Al_2O_3–SiO_2–H_2O System at the transition zone pressures. Geophys Res Lett 28:1303–1306

Martirosyan N et al (2016) The $CaCO_3$–Fe interaction: kinetic approach for carbonate subduction to the deep Earth's mantle. Phys Earth Planet Inter 259:1–9

McCammon C (1997) Perovskite as a possible sink for ferric iron in the lower mantle. Nature 387:694–696

Melekhova E et al (2007) The composition of liquids coexisting with dense hydrous magnesium silicates at 11–13.5 GPa and the end-points of the solidi in the MgO–SiO_2–H_2O system. Geochimica et cosmochimica acta 71:3348–3360

Mibe K et al (2002) Composition of aqueous fluid coexisting with mantle minerals at high pressure and its bearing on the differentiation of the Earth's mantle. Geochim Cosmochim Acta 66:2273–2285

Morishima H et al (1994) The phase boundary between α-and β-Mg_2SiO_4 determined by in situ X-ray observation. Science 265:1202–1203

Ohtani E et al (1995) Melting relations of peridotite and the density crossover in planetary mantles. Chem Geol 120:207–221

Ohtani E, Suzuki A, Kato T (1998) Flotation of olivine and diamond in mantle melt at high pressure: implications for fractionation in the deep mantle and ultradeep origin of diamond. In: Manghnani MH, Yagi T (eds) Properties of Earth and planetary materials at high pressure and temperature. Geophysical monograph, vol 101. American Geophysical Union, Washington DC, 227–239

Ohtani E et al (2001) Stability of dense hydrous magnesium silicate phases and water storage capacity in the transition zone and lower mantle. Phys Earth Planet Inter 124:105–117

Ottonello G et al (2010) Thermo-chemical and thermo-physical properties of the high-pressure phase anhydrous B ($Mg_{14}Si_5O_{24}$): an ab-initio all-electron investigation. Am Miner 95:563–573

Palyanov YN et al (2013) Mantle–slab interaction and redox mechanism of diamond formation. Proc Natl Acad Sci 110:20408–20413

Ringwood A, Major A (1967) High-pressure reconnaissance investigations in the system Mg_2SiO_4–MgO–H_2O. Earth Planet Sci Lett 2:130–133

Rohrbach A, Schmidt MW (2011) Redox freezing and melting in the Earth/'s deep mantle resulting from carbon-iron redox coupling. Nature 472:209–212

Rohrbach A et al (2007) Metal saturation in the upper mantle. Nature 449:456–458

Smith EM et al (2016) Large gem diamonds from metallic liquid in Earth's deep mantle. Science 354:1403–1405

Stachel T et al (2000) Kankan diamonds (Guinea) II: lower mantle inclusion parageneses. Contrib Miner Petrol 140:16–27

Stalder R et al (2001) High pressure fluids in the system MgO–SiO_2–H_2O under upper mantle conditions. Contrib Miner Petrol 140:607–618

Suzuki A et al (2000) In situ determination of the phase boundary between wadsleyite and ringwoodite in Mg_2SiO_4. Geophys Res Lett 27:803–806

Xiong F et al (2015) Origin of podiform chromitite, a new model based on the Luobusa ophiolite, Tibet. Gondwana Res 27:525–542

Yang J-S et al (2007) Diamond-and coesite-bearing chromitites from the Luobusa ophiolite. Tibet Geology 35:875–878

Zhang Y et al (2013) Phase transitions of harzburgite and buckled slab under eastern China. Geochem Geophys Geosyst 14:1182–1199

Zhang Y et al (2016) Experimental constraints on the fate of subducted upper continental crust beyond the "depth of no return". Geochim Cosmochim Acta 186:207–225